Submitted to the 25th International Laser Radar Conference (ILRC)
5-9 July 2010, St. Petersburg, Russia

HORIZONTAL MOTION VECTORS FROM CROSS-CORRELATION: FIRST APPLICATION TO EYE-SAFE AEROSOL LIDAR DATA FROM CHATS

Shane D. Mayor

Department of Physics, California State University Chico
Chico, California, 95929, USA, E-mail: sdmayor@csuchico.edu

ABSTRACT

Results are presented from the application of the cross-correlation technique to data collected with an eye-safe ground-based scanning aerosol backscatter lidar at 1.5 microns wavelength. The resulting motion vectors are compared with sonic anemometer measurements collected from a tower located within the lidar scan area. This paper describes the image processing and numerical steps implemented thus far in a software program to compute the horizontal motion vectors from the aerosol lidar data and two comparisons of the resulting vectors with corresponding anemometer data. In one case spanning 2.5 hours, speed and direction are plotted every 17 s using lidar data from a 250×250 m^2 area during weakly stable and nearly quiescent evening conditions. In the other case spanning 3 hours, speed and direction are plotted every 30 s from a 500×500 m^2 area during more turbulent afternoon conditions and the passage of a density current front. While a previous study demonstrated comparable spatial resolution using a non-eye-safe lidar system, this paper shows higher temporal resolution results from an unattended lidar system that is eye-safe.

1. MOTIVATION

Remote measurements of the vector wind field in the atmospheric boundary layer from ground-based locations on the order of kilometers away from the area of interest are still needed in several applications. Examples include wind resource assessments and monitoring near established wind farms; determining the initial transport and dispersion of hazardous materials (i.e. nuclear power and industrial chemical sites); detecting wind shear and wake vortices near airports; and micro-meteorological research. Doppler lidars provide precise measurements of only the radial component of motion. In many of the above applications it is not practical to collect 360° azimuth scans or assume horizontal homogeneity of the atmospheric boundary layer, or combine radial measurements with numerical flow retrieval models, to derive two or more wind components. The use of two separated Doppler lidars simultaneously can provide multiple wind components over a common area, but this is likely to be a prohibitively expensive solution in many cases. Instead, a direct observation of two or more components of the vector wind field is desired from scanning over a sector with a single instrument. It is this scenario that the application of the cross-correlation technique to aerosol backscatter lidar images may hold significant value. A primary research objective of the project that resulted in this paper is to derive two-component horizontal wind vectors in the atmospheric surface layer from an eye-safe aerosol lidar and compare them with in situ measurements to determine the accuracy and reliability of the method.

2. BACKGROUND

The cross-correlation technique has been applied to aerosol lidar data several times previously [1–8]. It was also applied to weather radar data [9] and satellite images [10]. The most recent of these papers [8] showed two-component vector fields with 250 m horizontal resolution over areas as large as 60 km^2. These vectors however were the result of large amounts of temporal averaging of many cross-correlation functions—up to 41 minutes in one case. Furthermore, the lidar used in [8] was not eye-safe and the scans were not coincident with any independent forms of wind measurement for validation.

In the present work, no temporal averaging of the cross-correlation functions was performed. The data was collected with an eye-safe elastic lidar operating at 1.5 microns wavelength [11] and a micro-meteorological tower was located within the lidar scan plane. The lidar and in situ data were collected nearly continuously over three months. This data set enables a comprehensive evaluation of the technique that will be conducted over the next two years.

3. ALGORITHM

A new program has been developed in Interactive Data Language (IDL) to calculate the vectors using the correlation technique from the aerosol backscatter data. The following is a list of steps—most of which have been described in previous papers (as indicated). Boxes with check marks indicate the steps that have been implemented in the IDL program used to calculate the results presented in this paper. Open boxes indicate steps that were not implemented but may be in the future.

1. ☑ Calculate relative aerosol backscatter intensity from the raw lidar returns by (a) subtracting the mean background from each waveform; (b) multiplying by the square of the range to remove the one-over-range-squared dependence of the raw signal; and (c) converting to decibels.

2. ☑ Apply a rolling low-pass median filter with a very short window (7 data points) to remove single point outliers. These points are relatively infrequent, uncorrelated, and thought to be caused by insects.

3. ☑ Apply a rolling high-pass median filter to eliminate large scale features such as the effects of attenuation and the present inability to normalize for shot-to-shot laser pulse energy variations. In the work here, a 333-point window was used and data points were spaced every 1.5 m in range.

4. ☑ Interpolate the backscatter arrays in their native spherical coordinate system to a Cartesian grid. This step ("gridding") is implemented in the current program by use of the IDL polar_surface.pro function. The Cartesian grid-spacing is 10 m in both the x and y directions.

5. ☑ Interpolate time and signal-to-noise ratio data to Cartesian arrays so that this information can easily be extracted over the exact regions that the correlation technique will be applied to.

6. □ Calculate a temporal median image. That is, for each point in the Cartesian image, calculate the median over time.

7. □ Subtract the temporal median image from the images that will be used to compute the correlation function. This is to remove stationary features in the images. [7]

8. □ Correct for image distortion. [4]

9. ☑ Extract a region of interest from Cartesian grids from two scans. Extract the time and signal to noise ratio (SNR) data over the same region.

10. ☑ Apply histogram equalization to the set of points within the region. [7]

11. ☑ Calculate the two-dimensional cross-correlation function using fast-Fourier transforms.

12. ☑ Calculate a bicubic natural nonsmoothing spline to points of correlation function nearest its peak [7]. For this work, the 9×9 points nearest the coarse peak were used to calculate a 100×100 spline surface using subroutines from [12].

13. ☑ Locate the peak of the bicubic spline surface.

14. ☑ Determine the time separation between frames.

15. ☑ Calculate the average lidar SNR and the average image SNR of the block region (for analysis).

16. ☑ Calculate the velocity vector based on the displacement of the peak with respect to the origin of the correlation function.

4. RESULTS

The CHATS data set contains approximately 1850 hours of lidar data from approximately 77 days of nearly-continuous operation. Here, the algorithm described above was applied to just two cases thus far. Lidar scans, time-lapse animations, and in situ measurements of corresponding temperature and vertical velocity can be found in the paper presented at the 24th ILRC [13].

4.1. 21 March 2007: Weakly stable evening

The first case is from the evening of 21 March 2007 between 04:15 and 06:45 UTC. This 2.5 hour period occurred during the evening from about sunset until 15 minutes before midnight. During this time the atmospheric surface layer was weakly stable (z/L stability parameter at 12.5 m AGL was +0.035) and the winds were light (less than 2 m s^{-1} for the most part) and variable. The lidar was programmed to repeat a sequence of 40 consecutive PPI scans followed by 2 consecutive RHI scans. The PPI scans ranged from 150° to 210° azimuth at a scan rate of 4° s^{-1}. This resulted in one scan every 17.3 s. The lidar transmitted 10 pulses per s and digitized backscatter at 1.5 m intervals in range. The angular separation between beams was 0.4°.

Motion vectors were calculated from pairs of frames over a 250 x 250 m area of lidar backscatter data centered on the ISFF vertical tower that was located 1600 m directly south of the lidar site. Fig. 1 shows the speed (top panel) and direction (bottom panel) during the period from the lidar (black) and a sonic anemometer (red) from 12.5 m AGL on the tower—the height closest to the lidar scan plane at that range. The sonic anemometer data (sampled at 60 Hz) have been averaged over the time span required by the lidar to scan the region twice. Therefore, data points shown for both the lidar and in situ wind are every 17.3 s. The average SNR of the raw backscatter data over this region ranged from 63 to 166 during the period. The SNR of the images used to compute the cross-correlation functions ranged from 0.43 to 22 and had a median value of 1.8.

Time-lapse animations of the lidar images from this case show what appear to be a substantial amount of gravity wave activity and episodes of turbulence. The gravity wave propagation vector may not equal the local wind vector. A hypothesis of this research is that the correlation technique may fail during stable periods because it may track wave propagation. These results suggest that the correlation method is capable of good performance during weakly stable and light wind conditions with wave activity.

4.2. 26 April 2007: Afternoon sea-breeze front

The second case is from the afternoon between 22:00 UTC on 26 April and 01:00 UTC on 27 April 2007. The lidar was programmed to collect alternating RHI and PPI scans. This provided one PPI scan (or one RHI scan) every 30 s. The PPI scans were directed between 151° and 211° azimuth at a scan rate of 4° s^{-1}. As with the previous case, the lidar transmitted 10 pulses per second and digitized backscatter at 1.5 m intervals in range. The angular separation between beams was 0.4°.

During this period, a density current front passed over the experimental site at 23:25 UTC on 26 April. The z/L stability parameter at 12.5 m height ranged from –2.0 to –0.6 (strongly to moderately unstable) before the arrival

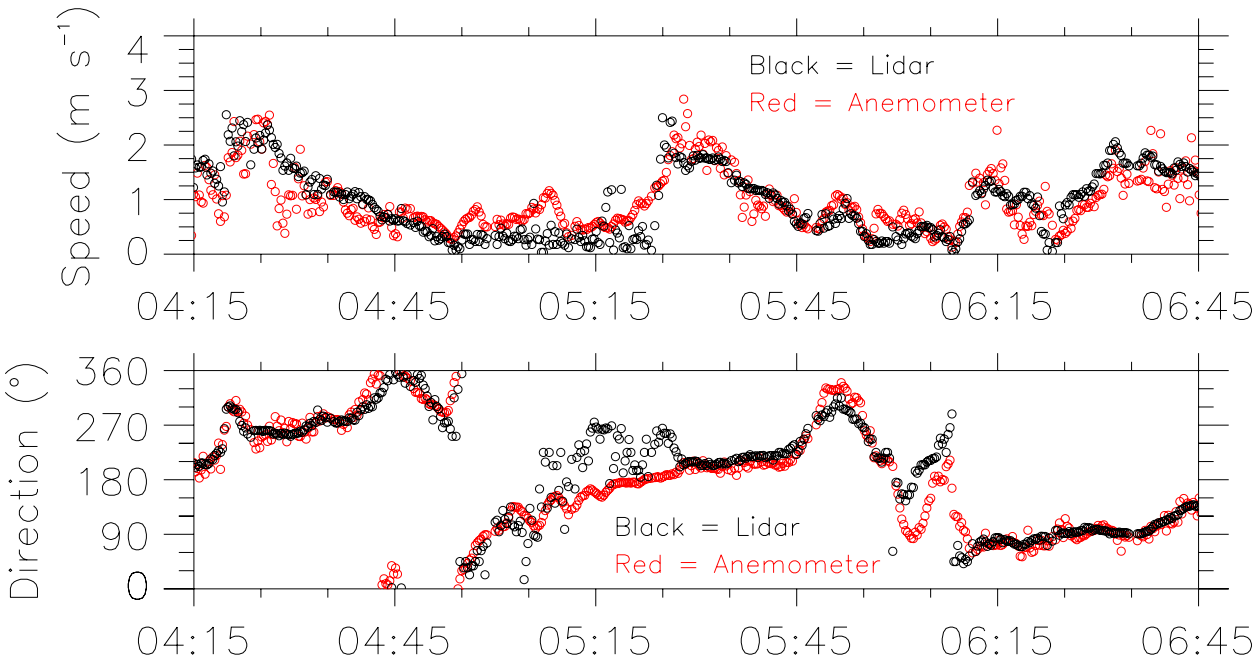

Figure 1: Comparison of wind speed (top) and direction (bottom) from sonic anemometer data (red) and the cross-correlation technique applied to the lidar data (black) over a 2.5-hour time span on the evening of 21 March 2007. During this period the atmosphere was weakly stable and the winds were light and variable. Lidar data points were calculated from 250 × 250 m^2 square regions centered on the ISFF tower from pairs of frames at 17.3 s intervals. Times are in UTC.

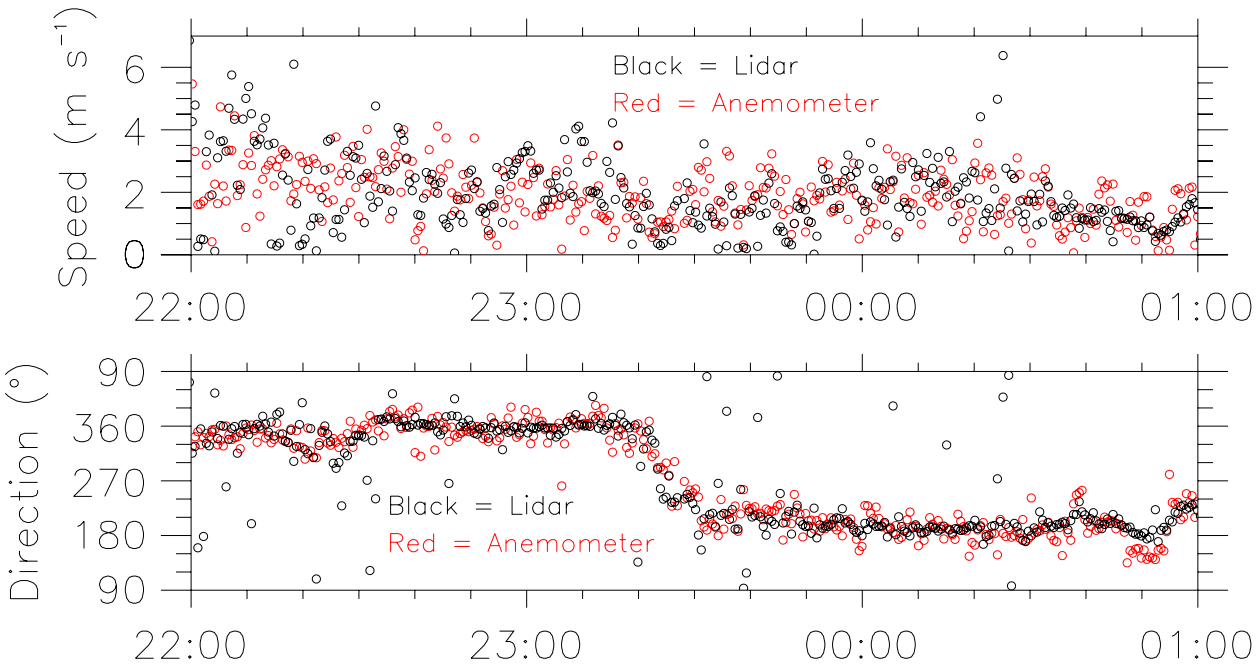

Figure 2: Comparison of wind speed (top) and direction (bottom) from sonic anemometer data (red) and the cross-correlation technique applied to the lidar data (black) over a 3-hour time span on the afternoon of 26–27 April 2007. During the middle of this period, a density current front passed over the experimental site approximately reversing the wind direction. Due to the collection of alternating PPI and RHI scans, the PPI frames used to calculate the motion were spaced in time at 30 s intervals. The algorithm used a 500 × 500 m^2 box centered around the tower supporting the sonic anemometer. Times are in UTC.

of the front and –0.5 to –0.2 (moderately to weakly unstable) after the passage of the front. During the entire period, wind speeds remained below approximately 4 m s^{-1}. However, the mean wind direction changed dramatically from 350° (N) before the front to 221° (SSW) after the front.

This case shows a substantial amount of scatter in both the anemometer wind speeds and the lidar wind speeds that is not present in the previous case. This difference is attributed to the more turbulent conditions of this case. However, the direction data appears to be in good agreement.

5. CONCLUSIONS

Mayor and Eloranta [8] presented motion vectors that were calculated by applying the cross-correlation technique to 250 x 250 m areas and averaging many correlation functions in time. In this paper, motion vectors were calculated from 250 $\times$ 250 m^2 and 500 $\times$ 500 m^2 areas from pairs of lidar scans and no time averaging of the correlation functions. These encouraging new results show that under some conditions it is possible to remotely measure changes in the wind speed and direction on time scales of approximately 1 minute or less and spatial scales of approximately 250 m resolution. In addition, the data presented here were collected with an eye-safe and unattended lidar system. In the future, the accuracy of the vectors will be explored as a function the lidar scan strategy, wind speed, static stability, turbulent kinetic energy, and SNRs of the raw data and gridded data after image processing.

The algorithm used here is not new. However, the lidar system and data set are new. Specifically, the lidar is capable of collecting high SNR backscatter returns from single pulses at 10 Hz with high range resolution. Moreover, it is eye-safe and can be operated unattended. These features, in combination with the coordinated in situ micro-meteorological data collection make evaluation of the cross-correlation technique feasible. In the near future, other algorithms currently under development [14–16] to extract vectors flow fields from the images may enable more robust two-component wind field information from single, eye-safe, scanning aerosol lidars.

ACKNOWLEDGMENTS

This work was made possible by Grant 0924407 from the U.S. National Science Foundation's Physical and Dynamic Meteorology Program.

REFERENCES

1. Eloranta, E. W., King, J. M. and Weinman, J. A. 1975: The determination of wind speeds in the boundary layer by monostatic lidar. *J. Appl. Meteor.*, **14**, pp. 1485–1489.
2. Sroga, J. T., Eloranta, E. W. and Barber, T. 1980: Lidar measurements of wind velocity profiles in the boundary layer. *J. Appl. Meteor.*, **19**, pp. 598–605.
3. Kunkel, K. E., Eloranta, E. W. and Weinman, J. 1980: Remote determination of winds, turbulence spectra and energy dissipation rates in the boundary layer from lidar measurements. *J. Atmos. Sci.*, **37**, pp. 978–985.
4. Sasano, Y., Hirohara, H., Yamasaki, T., Shimizu, H., Takeuchi, N. and Kawamura, T. 1982: Horizontal wind vector determination from the displacement of aerosol distribution patterns observed by a scanning lidar. *J. Appl. Meteor.*, **21**, pp. 1516–1523.
5. Hooper, W. P. and Eloranta, E. W. 1986: Lidar measurements of wind in the planetary boundary layer: the method, accuracy and results from joint measurements with radiosonde and kytoon. *J. Clim. Appl. Meteor.*, **25**, pp. 990–1001.
6. Kolev, I., Parvanov, O. and Kaprielov, B. 1988: Lidar determination of winds by aerosol inhomogeneities: motion velocity in the planetary boundary layer. *Appl. Optics*, **27**, pp. 2524–2531.
7. Schols, J. L. and Eloranta, E. W. 1992: The calculation of area-averaged vertical profiles of the horizontal wind velocity from volume imaging lidar data. *J. Geophys. Res*, **97**, pp. 18395–18407.
8. Mayor, S. D. and Eloranta, E. W. 2001: Two-dimensional vector wind fields from volume imaging lidar data. *J. Appl. Meteor.*, **40**, pp. 1331–1346.
9. Rinehart, R. E. and Garvey, E. T. 1978: Three-dimensional storm motion detection by conventional weather radar. *Nature*, **273**, pp. 287-289.
10. Leese, J. A., Novak, C. S. and Clark, B. B. 1971: An automated technique for obtaining cloud motion from geosynchronous satellite data using cross correlation. *J. Appl. Meteor.*, **10**, pp. 118–132.
11. Mayor, S. D., Spuler, S. M., Morley, B. M. and Loew, E. 2007: Polarization lidar at 1.54-microns and observations of plumes from aerosol generators. *Opt. Eng.*, **46**, DOI: 10.1117/12.781902.
12. Press, W. H., Flannery, B. P., Teukolsky, S. A. and Vetterling, W. T. *Numerical Recipes in FORTRAN 77: The Art of Scientific Computing*. Cambridge University Press, Cambridge, U.K., 1992.
13. Mayor, S. D. 2008: Observations of sea-breeze fronts and turbulence near the surface during stable conditions. *24th Int. Laser Radar Conf.*, SO30–01.
14. Corpetti, T., Mémin, E. and Perez, P. 2002: Dense estimation of fluid flows. *IEEE T. Pattern Anal.*, **24**, pp. 365–380.
15. Héas, P., Mémin, E., Papadakis, N. and Szantai, A. 2007: Layered estimation of atmospheric mesoscale dynamics from satellite imagery. *IEEE T. Geosci. Remote.*, **45**, pp. 4087–4104.
16. Dérian, P., Héas, P., Mémin, E. and Mayor, S. D. 2010: Dense motion estimation from eye-safe aerosol lidar data. *25th Int. Laser Radar Conf.*